Research Square

Preprints are preliminary reports that have not undergone peer review.
They should not be considered conclusive, used to inform clinical practice,
or referenced by the media as validated information.

Transcriptome and metabolome analysis reveals time-staged flavonoid reprogramming in Curcuma alismatifolia roots under salt stress

Zhuo Wei
Yunnan University
Hong Zhao
Guizhou University of Engineering Science
Yingdie Yang
Guizhou University of Engineering Science
Yang Wang
Guizhou University of Engineering Science
Zuhong Fan
Guizhou University of Engineering Science
Tian Tian
Guizhou University of Engineering Science
Ying Deng
dy3594142@163.com
Guizhou University of Engineering Science

Research Article

Keywords: Curcuma alismatifolia, salt stress, transcriptome, metabolome, flavonoids, transcription factors

Posted Date: November 23rd, 2026

DOI: https://doi.org/10.21203/rs.3.rs-11633500/v1

License: This work is licensed under a Creative Commons Attribution 4.0 International License.
Read Full License

Additional Declarations: No competing interests reported.

Transcriptome and metabolome analysis reveals time-staged flavonoid reprogramming in *Curcuma alismatifolia* roots under salt stress

Zhuo Wei[1], Hong Zhao[2], Yingdie Yang[2], Yang Wang[2], Zuhong Fan[2], Tian Tian[2], Ying Deng[2*]

1.College of Ecology and Environment, Yunnan University, Kunming 650091, Yunnan, China

2.College of Ecological Engineering, Guizhou University of Engineering Science, Bijie 551700, Guizhou, China

Zhuo Wei: weizhuo1996@163.com

Hong Zhao: zhaohonggzu@163.com

Yingdie Yang: yingdiey2@163.com

Yang Wang: wangyang@gues.edu.cn

Zuhong Fan: fanzuhong@gues.edu.cn

Tian Tian: tiantian@gues.edu.cn

Ying Deng：dy3594142@163.com

Abstract

Soil salinization increasingly threatens ornamental crop production, yet the molecular mechanisms underlying salt responses in ornamental geophytes remain poorly understood. Transcriptome and metabolomics were used to characterize root responses of *Curcuma alismatifolia* to 100 mM NaCl at 24 h and 48 h. Transcriptome analysis identified 1599 differentially expressed genes at 24 h, with 1057 up-regulated and 542 down-regulated, and 4991 at 48 h, with 1496 up-regulated and 3495 down-regulated, revealing a shift from transcriptional activation to repression as stress persisted. Metabolome profiling detected 713 and 362 differentially accumulated metabolites at the two time points, showing a transient early accumulation of flavonol aglycones and monoglycosides and of phenylpropanoid conjugates, followed by accumulation of diglycosylated flavonoids at 48 h. KEGG enrichment identified phenylpropanoid biosynthesis, flavonoid biosynthesis as the terms consistently enriched in both omics layers at both time point. WGCNA analysis identified salt-responsive co-expression modules and screened the transcription factors *HSF8*, *NAC48*, *C3H2*, *HOX16* and *PER12* as candidate genes associated with flavonoid metabolism. RT-qPCR confirmed the RNA sequencing expression patterns of these genes. These findings characterize a time-staged

transcriptional and metabolic response to salt stress in this ornamental geophyte and provide candidate salt-responsive genes for further functional studies.

Keywords: *Curcuma alismatifolia*; salt stress; transcriptome; metabolome; flavonoids; transcription factors

Introduction

Soil salinization is one of the most widespread environmental factors limiting plant growth, development, and agricultural productivity worldwide, and its continuously expanding footprint poses an escalating threat to crop yields and global food security [1, 2]. When the salt concentration in soil is high, the soil water potential decreases and becomes more negative, which makes it difficult for plant roots to absorb water and thereby imposes osmotic stress [3]. In addition, excessive Na^+ accumulation in plant cells causes ion toxicity and disrupts normal physiological and biochemical processes [4, 5]. Because plants cannot escape salt stress, they have evolved specific tolerance mechanisms, such as Na^+ extrusion and vacuolar compartmentalization through the Salt Overly Sensitive pathway [6], osmotic adjustment via compatible solutes [7], and enhanced antioxidant capacity [8]. Most of these responses are governed by complex transcriptional and hormonal regulatory networks, and among the metabolic branches recruited by these networks under abiotic stress, flavonoid metabolism occupies a recurring position.

Flavonoids are common secondary metabolites in plants and are closely related to stress tolerance. Salt stress can significantly alter the expression levels of genes related to flavonoid biosynthesis, including chalcone synthase, CHS, flavanone 3-hydroxylase, F3H, and flavonol synthase, FLS, leading to the accumulation of antioxidant flavonoids such as luteolin and dihydroquercetin [9]. Overexpression of *CHS* and *FLS* genes has been shown to increase flavonoid content and improve salt tolerance in transgenic plants, indicating that up-regulation of key flavonoid-pathway genes, alone or in combination, can enhance stress resistance.

Integrating differentially expressed genes, DEGs, with differentially accumulated metabolites, DAMs, has proven effective for identifying the regulatory modules underlying salt tolerance [10, 11]. Complementing this multi-omics approach, transcription factor, TF, families such as WRKY, MYB, NAC, and basic leucine zipper, HOX16, have been identified as key upstream regulators of salt-stress responses [12]. *C. alismatifolia* is a ornamental geophyte of the family

Zingiberaceae, valued for its showy pink-to-white bracts and long vase life, and it is widely cultivated as a cut flower and potted plant in Southeast Asia and southern China. The molecular mechanisms by which *C. alismatifolia* responds to salt stress, however, remain poorly understood. In this study, transcriptome sequencing and untargeted LC–MS/MS metabolite profiling were performed on *C. alismatifolia* roots after 100 mM NaCl treatment for 24 h and 48 h, following a K^+ and Na^+ content pre-screen of 50 mM and 100 mM treatments. we further asked whether the salt-induced flavonoid program in this species is time-staged and whether it can be linked to identifiable transcriptional regulators.

Materials and methods

Plant materials, salt stress treatments, and ion content determination. This study used *C. alismatifolia* plants propagated from rhizomes and grown in plastic pots 18 cm in diameter filled with peat and perlite at a 3:1 volume ratio, in a greenhouse in Kunming, Yunnan Province, China, under a photoperiod of 14 h light and 10 h dark, an average temperature of 25 ± 2 °C, and a relative humidity of 60–70%, with Hoagland nutrient solution supplied every 7 days. When the plants reached the vegetative stage with 4 to 6 leaves, the substrate was irrigated with 50 mM or 100 mM NaCl solution, while plants irrigated with an equal volume of water served as the control, designated CK; each treatment comprised six pots arranged in a randomized complete block design. To determine an appropriate treatment concentration, root samples of the three groups were harvested after 24 h for K^+ and Na^+ determination. Because the two concentrations disrupted K^+/Na^+ homeostasis to a comparable extent whereas 100 mM imposed a higher salinity level, 100 mM was selected, and roots of the CK and treated plants were collected at 24 h and 48 h. For each of the four groups CK_24h, NaCl_24h, CK_48h, and NaCl_48h, three biological replicates were randomly taken, immediately frozen in liquid nitrogen, and stored at −80 °C, yielding 12 samples for transcriptome and metabolome analyses. For ion determination, root samples were heat-inactivated at 105 °C for 30 min, dried at 80 °C to constant weight, and ground to powder. Dry samples of 0.1 g were digested with H_2SO_4–H_2O_2, and the K^+ and Na^+ concentrations of the digested solutions were determined with a flame photometer, from which the K^+/Na^+ ratio was calculated for each sample.

Transcriptome sequencing and data analysis

Total RNA was extracted from root samples using the TransZol Up Plus RNA Kit (TransGen Biotech, Beijing, China) following the manufacturer's instructions. RNA integrity and contamination were assessed by agarose gel electrophoresis, concentration was measured with a Qubit 2.0 Fluorometer (Thermo Fisher Scientific, Waltham, MA, USA), and the RNA integrity number, RIN, was determined on an Agilent 2100 Bioanalyzer (Agilent Technologies, Santa Clara, CA, USA); only samples with a RIN of at least 7.0 and an A260/230 ratio above 1.8 were used for library preparation. Libraries were constructed with the NEBNext Ultra RNA Library Prep Kit (New England BioLabs, Ipswich, MA, USA), assessed for insert size on the Agilent 2100 Bioanalyzer, and quantified by quantitative PCR to confirm effective concentrations above 2 nM before sequencing on the Illumina NovaSeq 6000 platform with 150 bp paired-end reads. After quality filtering, clean reads were mapped to the C. alismatifolia reference genome using HISAT2 v2.1.0 [13], gene-level read counts were obtained with featureCounts v1.6.2 [14], and fragments per kilobase of transcript per million mapped reads, FPKM, values were calculated for expression visualization. Differential expression analysis was performed with DESeq2 version 1.38.3 [15] on raw read counts; raw P values were adjusted by the Benjamini–Hochberg procedure to obtain the false discovery rate, FDR, and DEGs were identified with an absolute log2 fold change, log2FC, of at least 1 and an FDR below 0.05. DEGs from 24 h and 48 h were classified into time-point-specific and shared categories, principal component analysis and hierarchical clustering of the union DEGs were performed in R, and Venn diagrams were generated in R v4.2.1 with the VennDiagram package v1.6.20. Pathway enrichment was based on the Kyoto Encyclopedia of Genes and Genomes, KEGG [16], database, in which hypergeometric tests with Benjamini–Hochberg correction identified pathways significantly enriched among DEGs relative to the entire genome background.

Untargeted metabolomics analysis

Root samples were freeze-dried in a lyophilizer (Scientz-100F, Ningbo Scientz, China) and ground at 30 Hz for 1.5 min with a grinder (MM 400, Retsch); 100 mg of powder was extracted with 1 mL of 70% methanol, and the mixture was vortexed for 30 s at 30 min intervals over six cycles, incubated at 4 °C overnight, and centrifuged at 12,000 × g for 10 min, after which the supernatant was filtered through a 0.22-μm membrane for LC–MS/MS analysis. Untargeted profiling was performed on a Vanquish ultra-high-performance liquid chromatography system

coupled with a Q Exactive HF Orbitrap mass spectrometer (Thermo Fisher Scientific); chromatographic separation on an ACQUITY BEH C18 column of 2.1 × 100 mm, 1.7 μm, at 40 °C used water containing 0.1% formic acid and acetonitrile as mobile phases at 0.4 mL/min, and data were acquired in both positive and negative electrospray ionization modes. Quality control samples, pooled from equal volumes of all extracts, were inserted every 10 samples to monitor system stability and repeatability. Raw data were processed with XCMS [17] for peak detection, alignment, and normalization, yielding 5,578 features across the 12 samples, and metabolites were putatively annotated by matching accurate masses and MS/MS spectra against mzCloud, MassBank, KEGG, and HMDB; features at Metabolomics Standards Initiative level 3 were retained. Metabolites with an absolute log2FC of at least 1 and $P < 0.05$ in a two-tailed Student's t-test between the control and treated groups were considered DAMs; their relative abundances were z-score normalized for hierarchical clustering, and KEGG enrichment was performed with the hypergeometric test and Benjamini–Hochberg correction.

WGCNA and construction of the TF–flavonoid regulatory network

The gene expression matrix was constructed from the FPKM values of all 12 samples, and genes whose FPKM was below 1 in more than half of the samples were removed before weighted gene co-expression network analysis, WGCNA [18], was performed using the WGCNA package v1.70-3 in R. Network topology was evaluated across a range of soft-thresholding powers with the pickSoftThreshold function, and a soft-thresholding power of 9 was selected because it yielded a scale-free fit index above 0.8; modules were then identified with the blockwiseModules function using default parameters. The salt treatment traits Salt_24h and Salt_48h and the four flavonoid-related traits flavonoid, flavone, anthocyanin, and phenylpropanoid were used as association traits for module–trait correlation analysis. Genes whose module membership, defined as the correlation of a gene with its module eigengene, exceeded 0.8 in absolute value and whose gene significance exceeded 0.7 were screened as candidate hub genes. Salt-responsive differentially expressed TFs were then correlated with differentially expressed flavonoid and phenylpropanoid structural genes to construct a TF–flavonoid regulatory network, which was visualized using Cytoscape 3.9.1 [19].

RT-qPCR analysis

To verify the transcriptomic data, four TFs were selected, namely the heat shock factor gene

Chr03HB1513, hereafter *HSF*; the *NAC* gene *Chr12HB483*; the zinc finger gene *Chr10HA456*, hereafter *ZF*; and the *HOX16* gene *Chr15HB1267*; together with two phenylpropanoid-related genes, the peroxidase gene *PER12*, hereafter *PER12*, and *CAD5*. Total RNA was extracted from the same root samples used for RNA sequencing, RNA-seq, and first-strand complementary DNA was synthesized using the TransScript One-Step gDNA Removal and cDNA Synthesis SuperMix (TransGen Biotech, Beijing, China). Primers were designed using Beacon Designer (PREMIER Biosoft, Palo Alto, CA, USA), and their sequences are listed in Table S1. Actin served as the internal reference gene, and amplification was performed with PerfectStart SYBR qPCR SuperMix (TransGen Biotech, Beijing, China) on an ABI Prism 7500 instrument (Applied Biosystems, USA). Relative expression levels were calculated using the $2^{-}\Delta\Delta Ct$ method [20].

Data analysis and statistics. K^+ and Na^+ contents and RT-qPCR data were analyzed using Excel 2019 (Microsoft Corp., Redmond, WA, USA) and SPSS 26.0 for Windows (IBM Corp., Armonk, NY, USA). Significant differences were determined by one-way analysis of variance, and results with $P < 0.05$ were considered statistically significant; different lowercase letters indicate significant differences between groups at the 0.05 level, while the same letter indicates no statistically significant difference.

Results

K^+ and Na^+ contents and selection of the NaCl treatment concentration

To select an appropriate NaCl concentration for the subsequent time-course transcriptomic and metabolomic analyses, root K^+ and Na^+ contents were determined after 24 h of treatment with 0 (CK), 50, and 100 mM NaCl (Fig. 1A–C). Both NaCl treatments significantly elevated the K^+ content relative to the CK, with the highest value at 50 mM and a moderate but significant elevation at 100 mM (Fig. 1A). Na^+ content increased under both concentrations and was significantly higher at 100 mM than at 50 mM (Fig. 1B). Correspondingly, the K^+/Na^+ ratio decreased significantly in both treatments relative to the CK and was significantly lower at 100 mM than at 50 mM (Fig. 1C). Because 100 mM imposed the stronger perturbation of K^+/Na^+ homeostasis, it was selected as the treatment concentration for the subsequent analyses.

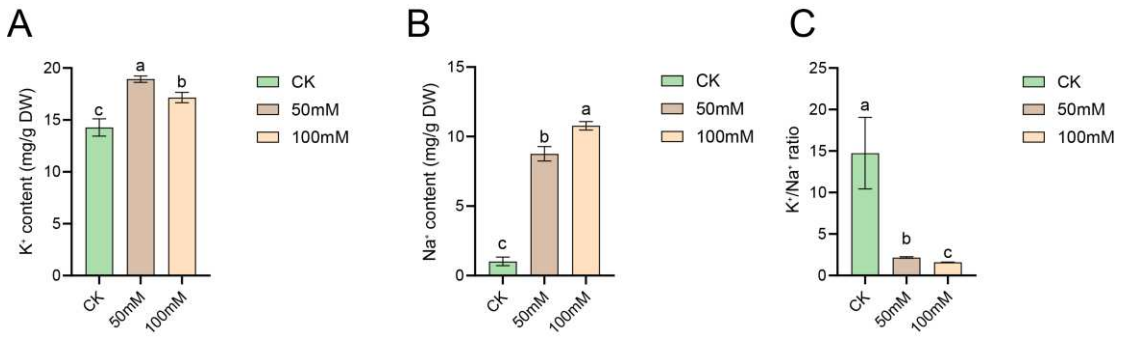


Fig. 1. Changes in K^+ and Na^+ contents and K^+/Na^+ homeostasis of *C. alismatifolia* under different NaCl treatments. A. K^+ content under the CK, 50 mM NaCl, and 100 mM NaCl treatments. B. Na^+ content under the three treatments. C. K^+/Na^+ ratio under the three treatments. Data are presented as means ± SD for n = 3. Different lowercase letters above the bars indicate significant differences at the 0.05 level with $P < 0.05$, while the same letters indicate no statistically significant differences.

Transcriptomic responses of *C. alismatifolia* roots to salt stress

To characterize the molecular basis of the salt-stress response under the selected 100 mM NaCl treatment, transcriptomes of *C. alismatifolia* roots were profiled under CK and NaCl-treated conditions at 24 h and 48 h. PCA revealed clear separation between the CK and NaCl groups at both time points, with the first two principal components, PC1 and PC2, accounting for 60.3% and 18.0% of the total variance respectively, indicating substantial transcriptional differences across treatments and high reproducibility within groups (Fig. 2A). Applying the thresholds of an absolute log2FC of at least 1 and an FDR below 0.05, 1599 DEGs were identified at 24 h, in which up-regulated genes, numbering 1057, substantially exceeded down-regulated ones, which numbered 542; at 48 h this pattern was reversed, as down-regulated genes, numbering 3495, far exceeded up-regulated ones, which numbered 1496, among 4991 DEGs in total. This reversal suggests a shift of the salt-stress response from transcriptional activation to repression as stress persisted. In addition, 9706 DEGs were detected between the two NaCl time points, including 3896 up-regulated and 5810 down-regulated genes, reflecting progressive transcriptional reprogramming during prolonged stress (Fig. 2C–E).

The DEGs were further classified into time-point-specific and shared categories (Fig. 2B). A total of 985 DEGs were commonly regulated at both time points, 635 of which were up-regulated and 345 down-regulated at both stages, whereas 614 and 4006 DEGs were exclusively

regulated at 24 h and 48 h respectively, showing that the late response was far more extensive than the early one. Hierarchical clustering of the 5605 union DEGs showed that the NaCl_48h group formed the most distinct cluster, while NaCl_24h occupied an intermediate position between the CK and NaCl_48h (Fig. 2F), consistent with the progressive intensification of the salt-stress response over time revealed by the DEG statistics.

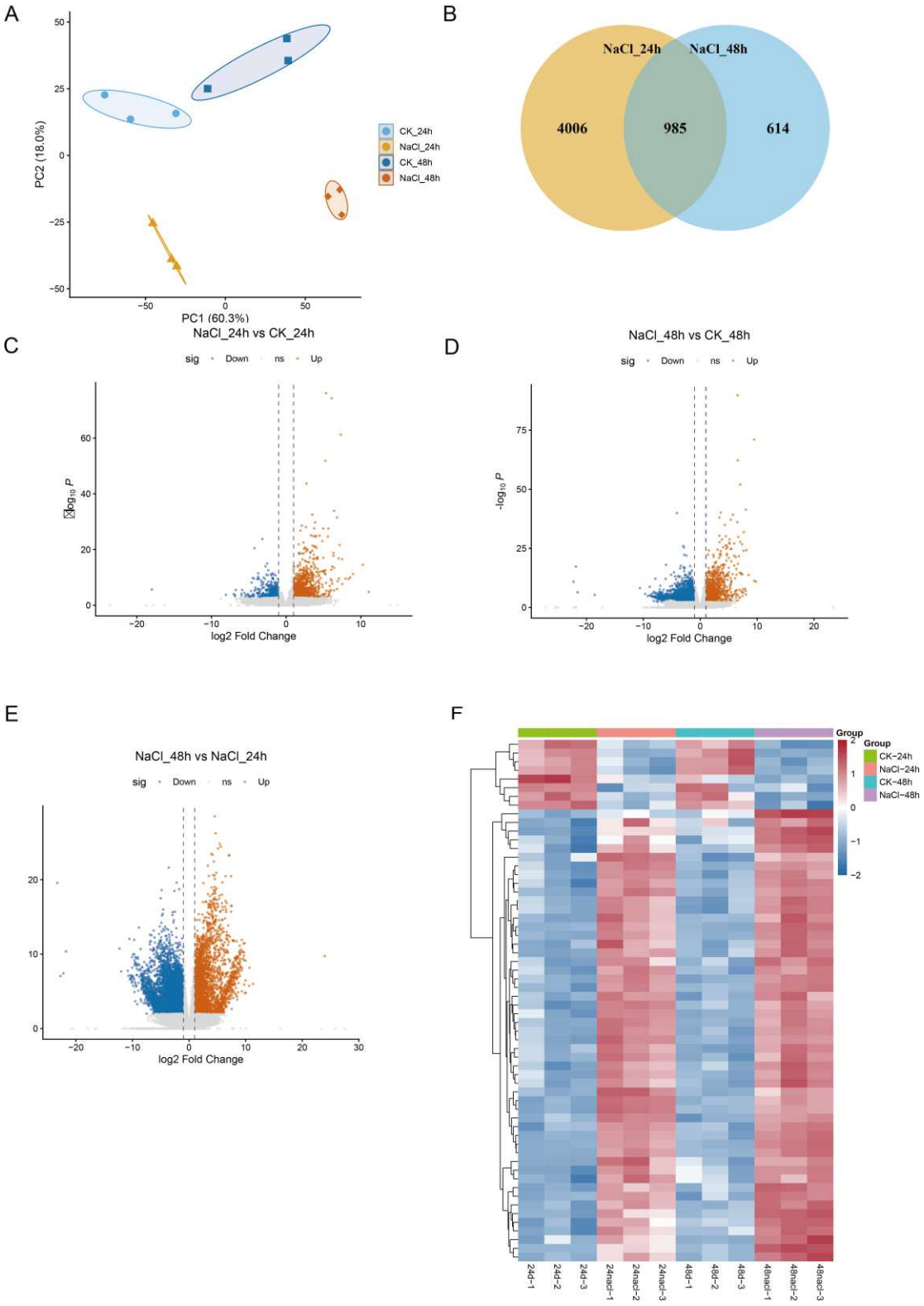


Fig. 2. Differentially expressed genes in *C. alismatifolia* roots under salt stress. A. Principal component analysis of the four groups CK_24h, NaCl_24h, CK_48h, and NaCl_48h; ellipses indicate within-group variation. B. Venn diagram of DEGs at the two time points; the overlap

represents DEGs commonly regulated by salt at both stages. C–E. Volcano plots of the NaCl_24h vs CK_24h, NaCl_48h vs CK_48h, and NaCl_48h vs NaCl_24h comparisons; blue, significantly down-regulated genes; red, significantly up-regulated genes; grey, non-DEGs. F. Heatmap of DEG expression levels across the four groups; red, higher expression; blue, lower expression.

Metabolomic responses of C. alismatifolia roots to salt stress

Untargeted LC–MS/MS profiling resolved 5578 features across the 12 samples, and PCA of all features separated the NaCl-treated samples from the time-matched controls at both 24 h and 48 h (Fig. 3A), mirroring the transcriptomic separation described above. Relative to the controls, 713 DAMs were detected at 24 h, of which 400 increased and 313 decreased in abundance, and 362 DAMs were detected at 48 h, of which 168 increased and 194 decreased; the time-course contrast of 48 h against 24 h yielded a further 910 DAMs, of which 391 increased and 519 decreased. The union of the three contrasts comprised 1420 features, yet only 72 DAMs were shared by the two treatment contrasts and 641 were unique to 24 h (Fig. 3B–E), indicating extensive turnover rather than progressive accumulation of the early metabolic response.

Classifying these DAMs into metabolic classes revealed a temporal organization that paralleled the transcriptional shift (Fig. 3F). The early response was dominated by the 57 flavonoid-related features and the 53 phenylpropanoid conjugates, which accumulated transiently at 24 h: the flavonol aglycone kaempferol rose to a log2FC of 6.7, three quercitrin-annotated monoglycosides to 4.6 to 5.3, and the flavanonol pinobanksin to 6.8, while sinapate, syringin, chlorogenic acid, 5-O-caffeoylshikimic acid, p-coumaroylquinic acid, and feruloylagmatine were induced in parallel, as was the osmolyte betaine at 6.1. All of these metabolites largely returned toward baseline in the time-course contrast, with log2FC values between −4.2 and −7.1. The late response, in contrast, was characterized by more heavily modified forms: the diglycosylated quercetin 3-O-rhamnoside 7-O-glucoside reached a log2FC of 6.7 at 48 h, dihydrokaempferol reached 4.7, the arginine-derived N-acetyl-L-citrulline reached 7.6 at 48 h and 11.5 in the time-course contrast, and the hydroxycinnamic acid amide p-coumaroylagmatine reached 8.3, whereas the purine degradation product xanthine declined to −6.0. The metabolome therefore moved from a transient pulse of flavonol aglycones, monoglycosides, and hydroxycinnamoyl conjugates at 24 h toward diglycosylated flavonoids

and amino-acid-derived conjugates at 48 h, and this course matched the time-staged DEG pattern.

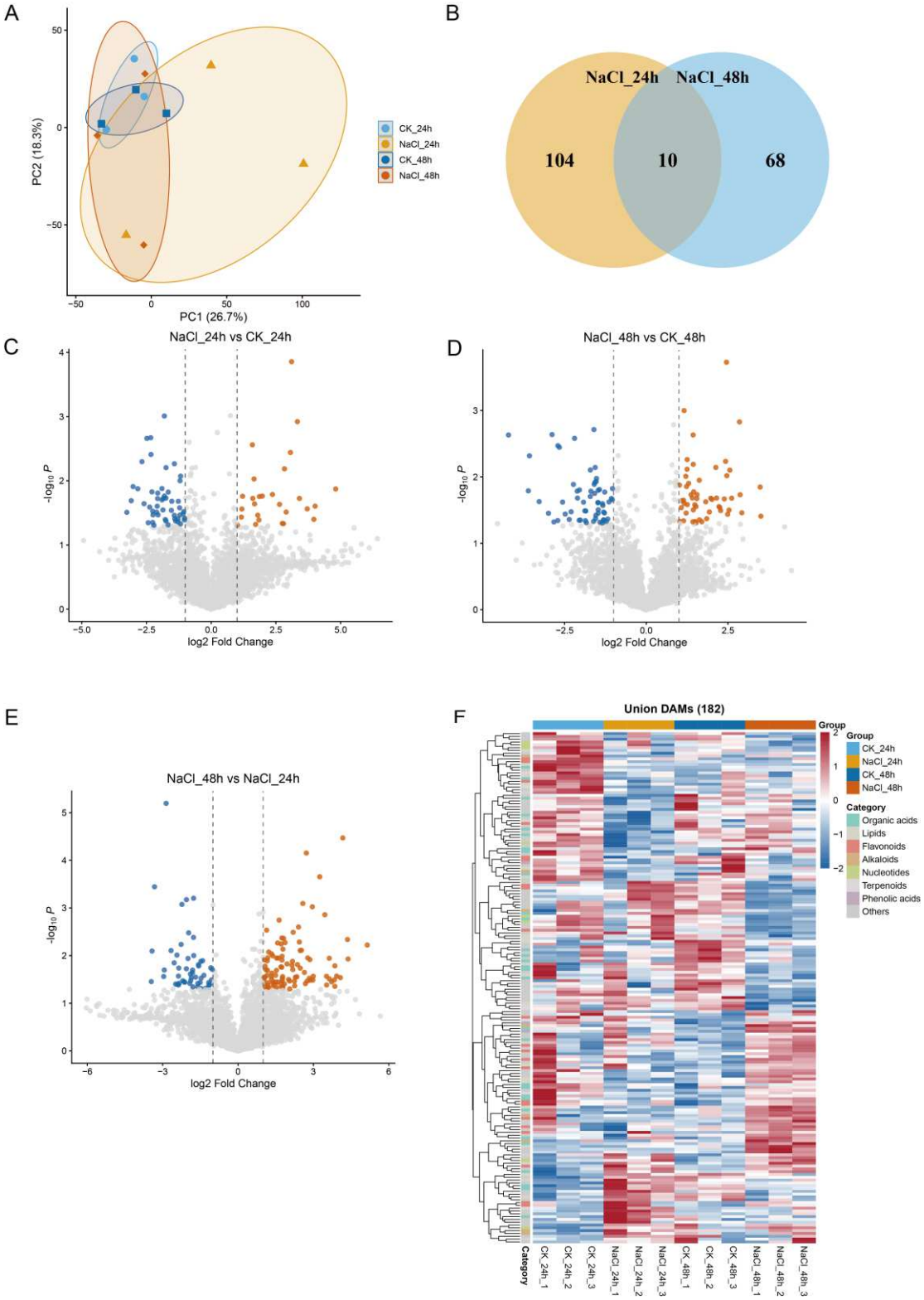


Fig. 3. Salt-induced remodeling of the root metabolome of *C. alismatifolia*. A. Principal component analysis of all 5578 z-scored LC–MS/MS features; three biological replicates per

group. B. Venn diagram of DAMs (absolute log2FC of at least 1, $P < 0.05$) between NaCl and control at 24 h and 48 h, numbering 713 and 362; 72 DAMs shared. C–E. Volcano plots of the NaCl vs control contrasts at 24 h and 48 h and the 48 h vs 24 h time-course contrast; dashed lines indicate DAM thresholds; Metabolomics Standards Initiative level 3-annotated compounds are labelled with feature IDs. F. Heatmap of z-scored intensities of 156 representative DAMs, comprising all 57 flavonoid-related DAMs, the seven glucosinolate-annotated features discussed below as likely annotation artifacts, and the most significant features of each remaining class; rows grouped by metabolic class with hierarchical clustering within classes; columns grouped by time point and treatment.

Integration of transcriptomic and metabolomic responses by KEGG enrichment analysis

To integrate the two omics layers, KEGG enrichment was performed on the DAMs (Fig. 4A) and the DEGs (Fig. 4B), and molecules annotated to the same pathway in both layers were taken to mark pathway-level salt responses jointly. Phenylpropanoid biosynthesis (ko00940), flavonoid biosynthesis (ko00941), plant hormone signal transduction (ko04075), starch and sucrose metabolism (ko00500), and purine metabolism (ko00230) were identified as the principal shared terms across the two omics layers. In the metabolome, flavone and flavonol biosynthesis (ko00944), and anthocyanin biosynthesis (ko00942) were specifically enriched at 24 h, as was glucosinolate biosynthesis (ko00966); cysteine and methionine metabolism (ko00270), tryptophan metabolism (ko00380), lysine biosynthesis (ko00300), and folate and one-carbon metabolism (ko00670, ko00790) were uniquely associated with the 48 h response. At the transcriptomic level, the mitogen-activated protein kinase signaling pathway in plants (ko04016), carotenoid biosynthesis (ko00906), zeatin biosynthesis (ko00908), and arginine and proline metabolism (ko00330) were specific to the early phase, while phenylpropanoid and flavonoid biosynthesis remained transcriptionally active at 48 h. Among all enriched terms, phenylpropanoid and flavonoid biosynthesis were therefore the only ones highlighted in both omics layers at both time points, and this convergence provided the rationale for the subsequent co-expression analysis focused on flavonoid-related traits.

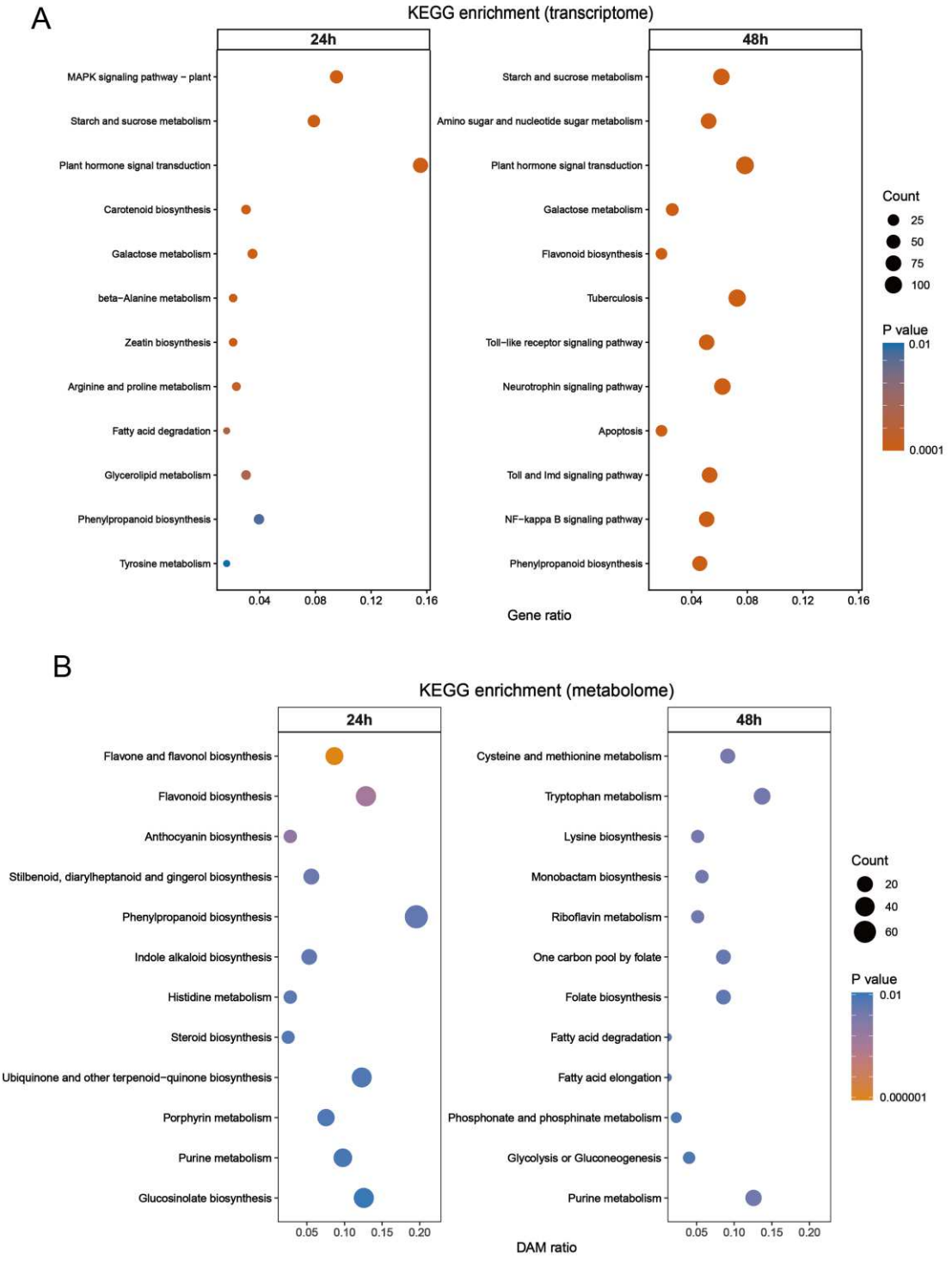


Fig. 4. KEGG enrichment of salt-responsive metabolites (A) and genes (B). A. Pathways overrepresented among DAMs at 24 h and 48 h by hypergeometric test with Benjamini–Hochberg correction; the 12 most significant pathways per contrast are shown; dot size, number of DAMs; color, raw P value on a log scale; the DAM ratio is the number of pathway DAMs divided by the pathway-mapped DAMs, 358 at 24 h and 175 at 48 h. B. Pathways enriched among DEGs at 24 h and 48 h; dot size, gene count; color, P value; the gene ratio is the number

of pathway DEGs divided by the total number of DEGs.

Identification of TFs associated with flavonoid metabolism by WGCNA and RT-qPCR validation

To identify TFs associated with the flavonoid metabolism highlighted in the preceding analyses, WGCNA was performed on the transcriptome expression matrix using the salt treatment traits Salt_24h and Salt_48h and the flavonoid-related traits as association traits. Hierarchical clustering showed that the samples separated by treatment and time point, with no obvious outliers (Fig. 5A). A total of 14 modules including the grey module were identified, and module–trait correlation analysis revealed that the MEblack module was significantly and positively correlated with Salt_24h at a coefficient of 0.85 as well as with most flavonoid-related traits, especially flavonoid, flavone, and anthocyanin, whereas MEblue was positively correlated with Salt_48h and negatively correlated with Salt_24h. The MEblack module was therefore considered functionally linked to the salt-induced flavonoid and phenylpropanoid response, and a TF–flavonoid regulatory network was constructed by correlating salt-responsive differentially expressed TFs with flavonoid and phenylpropanoid structural genes (Fig. 5C).

The network comprised the up-regulated TFs *HSF8*, *NAC48*, *C3H2*, and *HOX16*, the peroxidase gene *PER12*, and the down-regulated phenylpropanoid-related gene *CAD5*. Within the network, *HSF8*, *NAC48*, and *HOX16* were connected to multiple structural genes and served as putative hub nodes, suggesting TF-mediated transcriptional coordination of flavonoid and phenylpropanoid biosynthesis, whereas *CAD5* was linked to repressed branches, consistent with the partial suppression of the phenylpropanoid pathway. For RT-qPCR validation, these six genes were selected, and their expression trends under salt stress were largely consistent with the RNA-seq (Fig. 5D). *HSF* showed the strongest induction, followed by *HSF8*, *NAC48*, *HOX16* and *PER12*, whereas *CAD5* was consistently down-regulated, matching its role as a repressed node in the network.

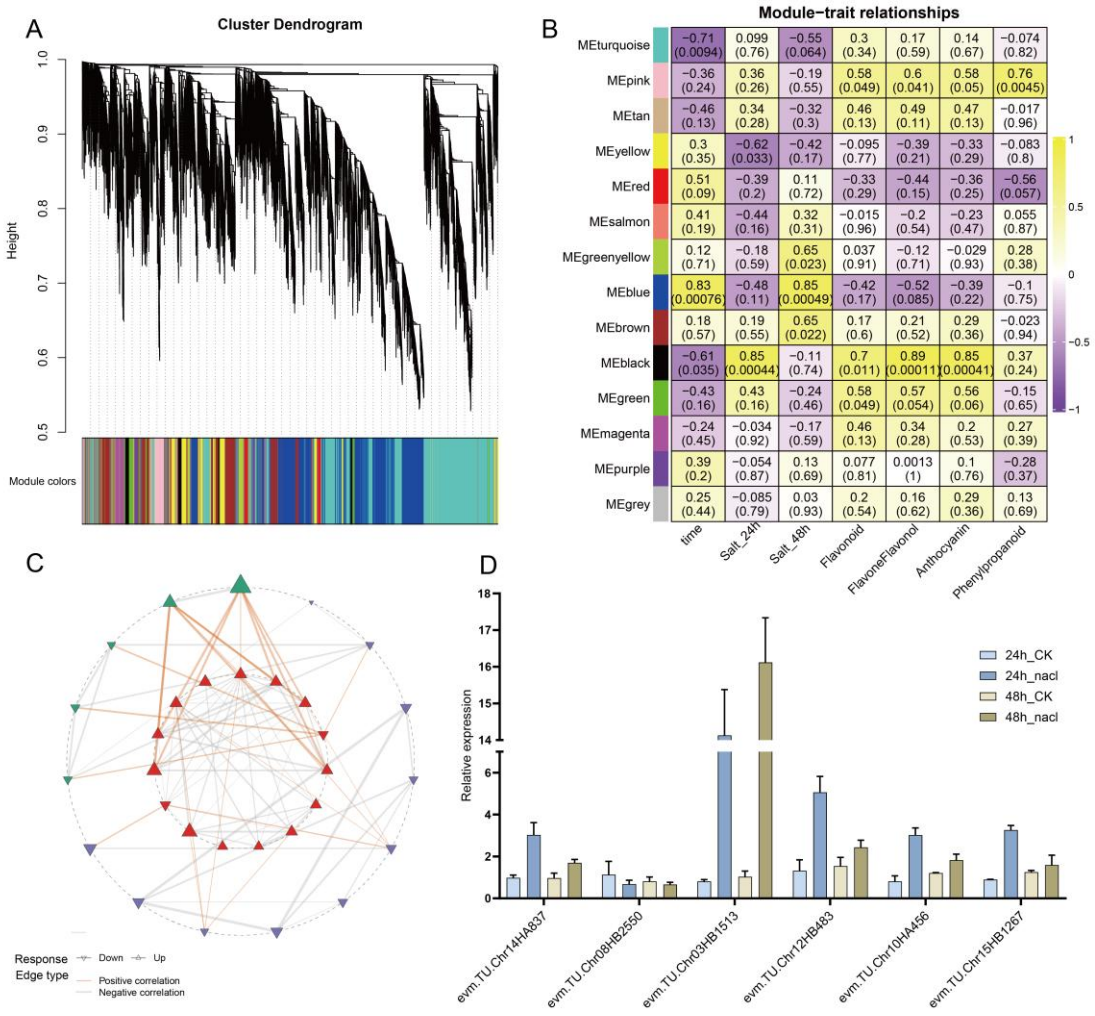


Fig. 5. WGCNA and RT-qPCR validation of flavonoid-related genes under salt stress. A. Sample clustering dendrogram of the transcriptome data. B. Module–trait correlations between the 14 modules and the salt treatment and flavonoid-related traits; cells show correlation coefficient and P value; red, positive; blue, negative. C. TF–flavonoid regulatory network of salt-responsive differentially expressed TFs and flavonoid and phenylpropanoid structural genes. D. RT-qPCR expression of six selected genes under CK, NaCl_24h, and NaCl_48h.

Discussion

In this study, we integrated ion determination, a NaCl concentration pre-screen, time-course transcriptome sequencing, and untargeted LC–MS/MS metabolomics to characterize the salt-stress response of *C. alismatifolia* roots over 24 to 48 h. The ionic measurements showed that K^+ content was significantly elevated under both NaCl concentrations, with the highest value at 50 mM, while Na^+ content also rose, so that the K^+/Na^+ ratio decreased significantly in both treatments and was lowest at 100 mM; K^+ retention and a high K^+/Na^+ ratio are recognized as

central determinants of salt tolerance [21, 22]. The concentration-screening strategy adopted here parallels that of a recent spelt study, in which a NaCl gradient from 0 to 200 mM was evaluated and 150 mM was selected as the concentration at which clear phenotypic divergence emerged [23]; in our case no phenotypic index was recorded, and 100 mM was chosen because it imposed the stronger perturbation of K^+/Na^+ homeostasis.

The time-course transcriptome showed a shift from activation-predominant transcriptional responses at 24 h to repression-predominant responses at 48 h. This predominance of down-regulated DEGs at 48 h resembles that reported in salt-stressed leaves of the tolerant faba bean genotype Hassawi-2, where down-regulated genes clearly outnumbered up-regulated ones after 72 h of 200 mM NaCl treatment, a pattern interpreted as conserving energy and resources by suppressing transcription [24]. This result is consistent with the growth–defense trade-off model, whereby plants attenuate growth to prioritize defense and survival [25].

Compared with the pronounced flavonoid accumulation reported for quinoa under saline–alkali stress [26], the flavonoid response of *C. alismatifolia* was transient at the level of aglycones and monosides and shifted toward more heavily glycosylated and conjugated forms at 48 h, exemplified by quercetin 3-O-rhamnoside 7-O-glucoside at a log2FC of 6.7. Glycosylation increases the solubility of flavonoids and facilitates their vacuolar sequestration [27], and UDP-glucosyltransferase-mediated redirection of metabolic flux has been implicated in abiotic stress tolerance in rice [28]. The late accumulation of the hydroxycinnamic acid amide p-coumaroylagmatine at a log2FC of 8.3, together with the early induction of feruloylagmatine, suggests the involvement of hydroxycinnamic acid amide metabolism, whose conjugation with alkylamines is an important component of salt-stress signaling [29].

KEGG enrichment identified phenylpropanoid biosynthesis, flavonoid biosynthesis, plant hormone signal transduction, starch and sucrose metabolism, and purine metabolism as the principal shared terms across the transcriptome and the metabolome. The early-specific enrichment of MAPK signaling is consistent with the role of MAPK cascades in relaying stress signals to downstream transcriptional activation [30] and with its recent identification as a principal salt-responsive KEGG term in pepper, where MAPK and hormone signaling were the most prominently enriched pathways in two species of contrasting salt tolerance [31]. The enrichment of plant hormone signal transduction, including zeatin biosynthesis, accords with

the documented involvement of phytohormone signaling in salt adaptation in wheat [32]. Among all enriched terms, phenylpropanoid and flavonoid biosynthesis were the only ones consistently highlighted in both omics layers at both time points, and this convergence provided the rationale for the co-expression analysis focused on flavonoid-related traits.

WGCNA identified the MEblack module as the one most strongly associated with salt treatment and flavonoid-related traits. In the TF–flavonoid network constructed here, the up-regulated *HSF8*, *NAC48*, *C3H2* factors emerged as putative hub-like nodes connected to multiple structural genes. The involvement of TF families in flavonoid regulation is well documented, with Arabidopsis *MYB111* binding the promoters of *CHS*, *F3H*, and *FLS1* to regulate flavonoid-mediated salt responses [33], *R2R3-MYB* overexpression increasing seedling flavonols [34], *NF-Y* contributing to flavonoid regulation in tomato [35], and *HOX16* factors functioning in ABA-mediated stress signaling [36]. Regarding structural genes, the peroxidase *PER12* was up-regulated whereas *CAD5* was repressed; given that individual class III peroxidases perform distinct functions [37], the coordinated regulation of these two genes suggests a differential recruitment of peroxidase-mediated phenylpropanoid metabolism during the salt response. RT-qPCR of six selected genes confirmed the RNA-seq patterns.

Conclusion

In this study, the salt-stress response of *C. alismatifolia* roots over 24 to 48 h of 100 mM NaCl treatment was characterized by joint transcriptome and metabolome analysis. Transcriptome analysis identified 1,599 DEGs at 24 h and 4991 DEGs at 48 h, revealing a shift from transcriptional activation, with 1057 up- and 542 down-regulated genes at 24 h, to transcriptional repression, with 1496 up- and 3,495 down-regulated genes at 48 h; metabolome profiling detected 713 and 362 DAMs, characterized by a transient early accumulation of flavonol aglycones and monoglycosides and of phenylpropanoid conjugates followed by the accumulation of diglycosylated flavonoids and amino-acid-derived metabolites at 48 h. Phenylpropanoid and flavonoid biosynthesis were the only terms highlighted in both omics layers at both time points, and WGCNA highlighted *HSF*, *NAC*, *ZF*, and *HOX16* as candidate hub regulators of flavonoid metabolism, with RT-qPCR confirming the expression patterns of six selected genes. Further transgenic validation of the candidate regulators, targeted quantification of phytohormones and key metabolites, and phenotypic damage assessment

across additional concentrations and genotypes will be required to verify these associations and to support the genetic improvement of salt tolerance in ornamental geophytes.

References

[1] Munns R, Gilliham M. Salinity tolerance of crops - what is the cost of heritability? New Phytologist. 2015; 208(3):668-673.

[2] Ma L, Li J, Li J, et al. Plant salt-tolerance mechanisms: Classic signaling pathways, emerging frontiers, and future perspectives. Molecular Plant. 2026; 19(3):538-570.

[3] Flowers TJ, Munns R, Colmer TD. Sodium chloride toxicity and the cellular basis of salt tolerance in halophytes. Annals of Botany. 2015; 115(3):419–431.

[4] Zhu JK. Abiotic stress signaling and responses in plants. Cell. 2016; 167(2):313-324.

[5] van Zelm E, Zhang Y, Testerink C. Salt Tolerance Mechanisms of Plants. Annual Review of Plant Biology. 2020; 71:403-433.

[6] Yang Y, Guo Y. Unraveling salt stress signaling in plants. Journal of Integrative Plant Biology. 2018; 60(9):796-804.

[7] Zhao C, Zhang H, Song C, et al. Mechanisms of Plant Responses and Adaptation to Soil Salinity. Innovation. 2020; 1(1):100017.

[8] Hasanuzzaman M, Raihan MRH, Masud AAC, et al. Regulation of reactive oxygen species and antioxidant defense in plants under salinity. International Journal of Molecular Sciences. 2021; 22(17):9326.

[9] Sharma A, Shahzad B, Rehman A, et al. Response of phenylpropanoid pathway and the role of polyphenols in plants under abiotic stress. International Journal of Molecular Sciences. 2019; 20(19):5045.

[10] Julkowska MM, Testerink C. Tuning plant signaling and growth to survive salt. Trends in Plant Science. 2015; 20(9):586-594.

[11] Alseekh S, Fernie AR. Metabolomics 20 years on: What have we learned and what hurdles remain? Trends in Plant Science. 2018; 23(6):551-558.

[12] Zhou H, Shi H, Yang Y, et al. Insights into plant salt stress signaling and tolerance. Journal of Genetics and Genomics. 2024; 51(1):16-34.

[13] Kim D, Paggi JM, Park C, et al. Graph-based genome alignment and genotyping with HISAT2 and HISAT-genotype. Nature Biotechnology. 2019; 37(8):907-915.

[14] Liao Y, Smyth GK, Shi W. featureCounts: An efficient general purpose program for assigning sequence reads to genomic features. Bioinformatics. 2014; 30(7):923-930.

[15] Love MI, Huber W, Anders S. Moderated estimation of fold change and dispersion for RNA-seq data with DESeq2. Genome Biology. 2014; 15(12):550.

[16] Kanehisa M, Goto S. KEGG: Kyoto encyclopedia of genes and genomes. Nucleic Acids Research. 2000; 28(1):27-30.

[17] Smith CA, Want EJ, O'Maille G, et al. XCMS: Processing mass spectrometry data for metabolite profiling using nonlinear peak alignment, matching, and identification. Analytical Chemistry. 2006; 78(3):779-787.

[18] Langfelder P, Horvath S. WGCNA: An R package for weighted correlation network analysis. BMC Bioinformatics. 2008; 9:559.

[19] Shannon P, Markiel A, Ozier O, et al. Cytoscape: A software environment for integrated models of biomolecular interaction networks. Genome Research. 2003; 13(11):2498-2504.

[20] Livak KJ, Schmittgen TD. Analysis of relative gene expression data using real-time quantitative PCR and the $2^{-\Delta\Delta Ct}$ method. Methods. 2001; 25(4):402-408.

[21] Assaha DVM, Ueda A, Saneoka H, et al. The role of Na^+ and K^+ transporters in salt stress adaptation in glycophytes. Frontiers in Physiology. 2017; 8:421.

[22] Ullah A, Ullah S, Arafat Y, et al. Endophytes-mediated mitigation of sodium stress in plants via ABA-independent signaling pathways. Plant Physiology and Biochemistry. 2025; 229(Pt B):110476.

[23] Zou S, Han G, Qie Y, et al. Transcriptome-level dissection provides unique insights into the salt tolerance in spelt (*Triticum spelta* L.). BMC Plant Biology. 2026; 26(1):1121.

[24] Afzal M, Alghamdi SS, Khan MA, et al. Transcriptomic analysis reveals candidate genes associated with salinity stress tolerance during the early vegetative stage in fababean genotype, Hassawi-2. Scientific Reports. 2023; 13:21223.

[25] Huot B, Yao J, Montgomery BL, et al. Growth-defense tradeoffs in plants: A balancing act to optimize fitness. Molecular Plant. 2014; 7(8):1267-1287.

[26] Wang M, Qi J, Li W, et al. Integration of transcriptome and metabolome provides insights into flavonoid biosynthesis in quinoa (*ChenoPER12ium quinoa* Willd.) responsive to saline-alkali stress. Plant Physiology and Biochemistry. 2025; 219:109988.

[27] Agati G, Azzarello E, Pollastri S, et al. Flavonoids as antioxidants in plants: Location and functional significance. Plant Science. 2012; 196:67-76.

[28] Dong NQ, Sun Y, Guo T, et al. UDP-glucosyltransferase regulates grain size and abiotic stress tolerance associated with metabolic flux redirection in rice. Nature Communications. 2020; 11(1):2629.

[29] Bassard JE, Ullmann P, Bernier F, et al. Phenolamides: Bridging polyamines to the phenolic metabolism. Phytochemistry. 2010; 71(14-15):1625-1637.

[30] Liu Y, Wang X, Lv H, et al. Anabolism and signaling pathways of phytomelatonin. Journal of Experimental Botany. 2022; 73(17):5801-5817.

[31] Farooq MA, Zeeshan Ul Haq M, Zhang L, et al. Transcriptomic insights into salt stress response in two pepper species: The role of MAPK and plant hormone signaling pathways. International Journal of Molecular Sciences. 2024;25(17):9355.

[32] Zamir H, Shah DA, Rauf F, et al. Salinity signaling networks in wheat: crosstalk among Ca^{2+}, ROS, phytohormones, and metabolic signals in salt adaptation. Plant Signaling Behavior. 2026; 21(1):2700909.

[33] Stracke R, Ishihara H, Huep G, et al. Differential regulation of closely related *R2R3-MYB* transcription factors controls flavonol accumulation in different parts of the *Arabidopsis thaliana* seedling. Plant Journal. 2007; 50(4):660-677.

[34] Mehrtens F, Kranz H, Bednarek P, et al. The Arabidopsis transcription factor *MYB12* is a flavonol-specific regulator of phenylpropanoid biosynthesis. Plant Physiology. 2005; 138(2):1083-1096.

[35] Wang J, Li G, Li C, et al. *NF-Y* plays essential roles in flavonoid biosynthesis by modulating histone modifications in tomato. New Phytologist. 2021; 229(6):3237-3252.

[36] Yoshida T, Fujita Y, Sayama H, et al. *AREB1*, *AREB2*, and *ABF3* are master transcription factors that cooperatively regulate *ABRE*-dependent ABA signaling involved in drought stress tolerance and require ABA for full activation. Plant Journal. 2010;61(4):672-685.

[37] Cosio C, Dunand C. Specific functions of individual class III peroxidase genes. Journal of Experimental Botany. 2009;60(2):391-408.

Author contributions

Zhuo Wei and Ying Deng designed the research. Zhuo Wei, Hong Zhao and Yingdie Yang

performed the experiments and data analysis. Yang Wang, Zuhong Fan and Tian Tian assisted with data curation. Zhuo Wei wrote the original manuscript. Ying Deng, Hong Zhao and Yingdie Yang revised the manuscript. All authors read and approved the final manuscript.

Data availability statement

The original contributions presented in the study are publicly available. This data can be found here: NCBI SRA, PRJNA1555209.

Funding

This work was supported by the Guizhou Provincial Science and Technology Projects (QKHJC-[2025]youth276).

Supplementary Files

This is a list of supplementary files associated with this preprint. Click to download.

- TableS1.xlsx